Proceedings of the 2022 International Conference on Smart Manufacturing and Material Processing (SMMP2022), A. Nayyar (Ed.)


doi:10.3233/ATDE220828

# Design and Simulation of Smart Bolt Based on Zno Piezoelectric Thin Film Sensor

Guowei MO [a,b], Yunxian CUI [a,1], Junwei YIN [a], Pengfei GAO [a] and Babak SAFAEI [c,d]
[a] *College of Mechanical Engineering, Dalian Jiaotong University, Dalian, People's Republic of China*
[b] *Department of Mechanical Engineering, Liaoning Machinery Electricity Vocational Technical College, Dandong, People's Republic of China*
[c] *Department of Mechanical Engineering, Eastern Mediterranean University, Famagusta, North Cyprus via Mersin 10, Turkey*
[d] *Department of Mechanical Engineering Science, University of Johannesburg, Gauteng, 2006, South Africa*

**Abstract:** In order to solve the coupling error problem of smart bolt, the coupling model of piezoelectric thin film sensor and bolt is established by using piezoelectric constitutive equation. The size parameters of ZnO piezoelectric film sensor are simulated and analyzed by finite element method using Comsol software M10× 1.5 piezoelectric thin film sensor is prepared on the bolt. First, the sensors of different piezoelectric materials are compared, and then the shape, size and thickness of the piezoelectric materials of the sensor are simulated; the size and thickness of electrode material are simulated. The simulation results show that the piezoelectric material is ZnO, the shape is round, the piezoelectric material size is 10mm, the piezoelectric thickness is 1000nm, the electrode material size is 6mm, and the electrode thickness is 200nm. ZnO piezoelectric thin film sensor was fabricated with this material and size.

**Keywords:** Smart bolt, piezoelectric thin film sensor, Comsol simulation, mathematical model, Finite element method, ZnO piezoelectric materials

## 1 Introduction

Piezoelectric sensors used to monitor the health of bolts are usually installed on the bolt surface or embedded in the bolt. At present, there are two common installation methods: adhesive and embedded structures.

[1] Corresponding author: Yunxian Cui, dlcyx007@126.com

According to the different positions where PZT patches are pasted, there are three common installation methods, as shown in Figure 1. The first is to paste PZT patch onto the bolt connection mechanism, mainly using ultrasonic measurement method[1-2], vibration analysis method[3-4], piezoelectric active sensing method[5-6] and electromechanical impedance method[7-8] to monitor the bolt looseness. The second is to paste PZT onto the washer to make smart washer [9-11], and identify the bolt looseness by monitoring the change of axial preload of the bolt. The third is to stick PZT patch to the bolt head, which can monitor the bolt looseness through ultrasonic time difference [12] or piezoelectric impedance change.

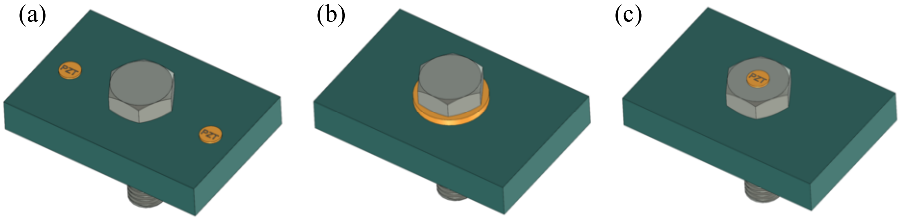


**Figure 1.** PZT paste method

Embedded structures are mainly divided into two types, as shown in Figure 2. The first method is to fabricate a groove on the bolt head to install the piezoelectric sensor inside, and monitor the pre tightening stress of the bolt using the acoustic elastic effect, as shown in Figure 2 (a) [13]. The second is embedded in the bolt, analyze the linear relationship between reflected Bragg wavelength and axial stress, and monitor the axial stress and shear stress of the bolt, as shown in Figure 2 (b) [14].

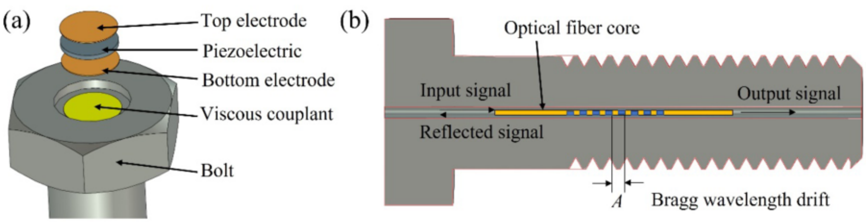


**Figure 2.** Two ways to embed sensors inside bolts

The connection methods of these methods and bolts are limited to the adhesive type and embedded type. The adhesive type connection will not only have the signal interference of the adhesive layer, but also will fall off over time due to the timeliness of the adhesive layer. In this paper, a new type of smart bolt based on ZnO piezoelectric film is proposed. The ZnO piezoelectric film sensor is directly deposited on the bolt head surface by using magnetron sputtering technology. According to the virtual work principle of elastic materials and the piezoelectric constitutive equation, the expression of the total potential energy of piezoelectric materials is written. In order to facilitate the calculation, the expression is converted to the polar coordinate form.

The extended Hamilton principle and Lagrangian function are used to deduce and transform the expression of the total potential energy of piezoelectric materials. Considering that the variation of variables in the expression is not affected by $\delta w(r,t)$ and $\delta D_3(r,t)$, the static coupling relationship between the potential shift $D_3(r,t)$ and the output voltage $V_a(r,t)$ can be obtained. The solid mechanical field and electrical field of the smart bolt are established by Comsol software, and the natural resonance frequency of the smart bolt is roughly scanned to confirm the approximate range of the admittance peak frequency. The design values of piezoelectric material, piezoelectric material shape, piezoelectric material size, piezoelectric material thickness, electrode material size and electrode thickness can be obtained through the simulation of each film layer of piezoelectric thin film sensor.

## 2. Design and mathematical model of intelligent bolt structure

### *2.1. Intelligent bolt structure*

According to the basic principle of piezoelectric effect, the smart bolt adopts sandwich structure, as shown in Figure 3.

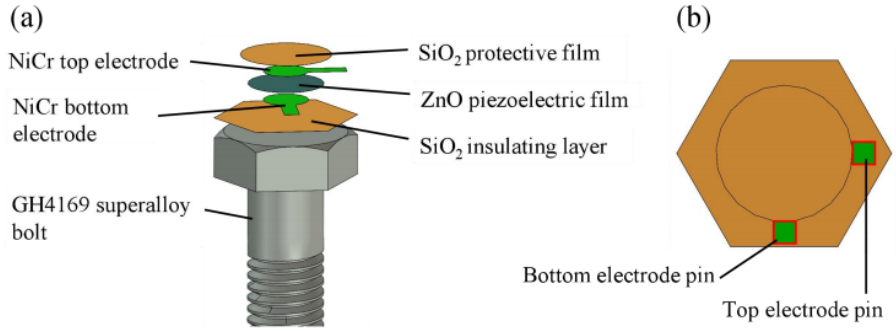


**Figure 3.** Structure diagram of ZnO PTFS of the smart bolt

### *2.2. Mathematical model of intelligent bolt*

The structural diagram of piezoelectric membrane smart bolt is shown in Figure 4. The piezoelectric membrane sensor is simplified as the piezoelectric layer is directly connected with the bolt head, and the binding force between them meets the bolt force requirements. The radius of the circular piezoelectric film sensor is $r_c$, Thickness is $h_c$, Bolt head radius $r_t$ thickness is $h_l$. For other details, please refer to Figure 4. The electric field generated by the piezoelectric film sensor is in the same direction as the stress deformation.

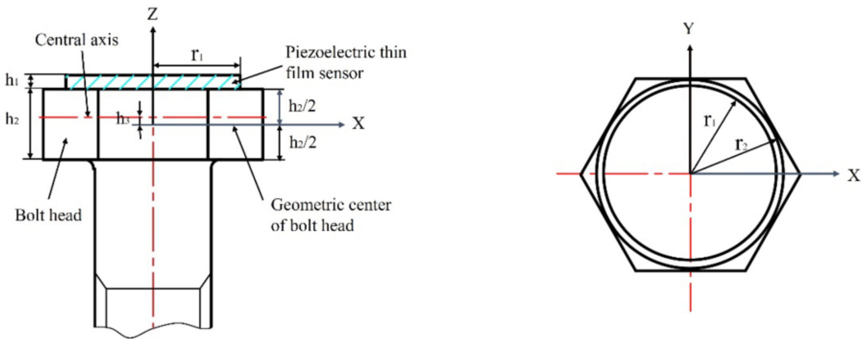


**Figure 4.** Schematic diagram of piezoelectric thin film smart bolt structure

In this paper, piezoelectric materials are discussed as linear materials. According to the virtual work principle of elastic materials, the total potential energy of piezoelectric body is expressed as:

$$\delta U = \int_V \left( \sigma_p \delta S_p + \in_i \delta D_i \right) dV \quad \left( i = 1,2,3;\ p = 1,2,\cdots,6 \right) \tag{1}$$

The piezoelectric constitutive equation is rewritten as:

$$\begin{cases} \sigma_p = c_{pq}^D S_q - h_{pi} D_i \\ \in_i = -h_{pi} S_p + \beta_{ij}^S D_j \end{cases} \tag{2}$$

Substitute Formula (2) into Formula (1) to get:

$$\delta U = \int_V \left\{ \left( c_{pq}^D S_q - h_{pi} D_i \right) \delta S_p + \left( -h_{pi} S_p + \beta_{ij}^S D_j \right) \delta D_i \right\} dV \quad \left( i = 1,2,3;\ p = 1,2,\cdots,6 \right) \tag{3}$$

For the circular piezoelectric film sensor, it is more convenient to use polar coordinates. The rectangular coordinates are converted into polar coordinates using geometric relations. The corresponding relations of coordinates are shown in Figure 5.

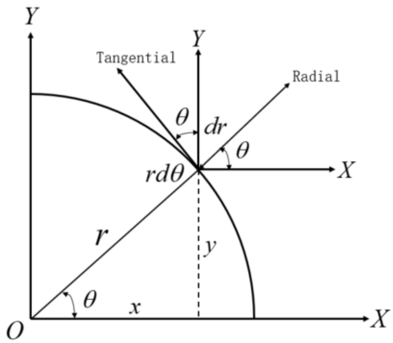


**Figure 5.** Schematic diagram of transformation between rectangular coordinate system and polar coordinate system

It can be seen from Figure 3 that:

$$\begin{cases} x = r\cos\theta,\ \ y = r\sin\theta \\ r^2 = x^2 + y^2,\ \ \theta = \tan^{-1}\dfrac{y}{x} \end{cases} \tag{4}$$

So we can get:

$$\begin{cases} \dfrac{\partial r}{\partial x} = \dfrac{x}{r} = \cos\theta,\ \ \dfrac{\partial r}{\partial y} = \dfrac{y}{r} = \sin\theta \\ \dfrac{\partial\theta}{\partial x} = \dfrac{\dfrac{\partial}{\partial x}\left(\dfrac{y}{x}\right)}{1+\dfrac{y^2}{x^2}} = -\dfrac{y}{x^2+y^2} = -\dfrac{\sin\theta}{r} \\ \dfrac{\partial\theta}{\partial y} = \dfrac{\dfrac{\partial}{\partial y}\left(\dfrac{y}{x}\right)}{1+\dfrac{y^2}{x^2}} = \dfrac{x}{x^2+y^2} = \dfrac{\cos\theta}{r} \end{cases} \tag{5}$$

The partial derivative of deflection $w$ to x and y can be written as the derivative form of $w$ to r and $\theta$:

$$\begin{cases} \dfrac{\partial w}{\partial x} = \dfrac{\partial w}{\partial r}\dfrac{\partial r}{\partial x} + \dfrac{\partial w}{\partial\theta}\dfrac{\partial\theta}{\partial x} = \cos\theta\dfrac{\partial w}{\partial r} - \dfrac{\sin\theta}{r}\dfrac{\partial w}{\partial\theta} \\ \dfrac{\partial w}{\partial y} = \dfrac{\partial w}{\partial r}\dfrac{\partial r}{\partial y} + \dfrac{\partial w}{\partial\theta}\dfrac{\partial\theta}{\partial y} = \sin\theta\dfrac{\partial w}{\partial r} + \dfrac{\cos\theta}{r}\dfrac{\partial w}{\partial\theta} \end{cases} \tag{6}$$

Therefore, it can be concluded that:

$$\begin{cases} \dfrac{\partial^2 w}{\partial x^2} = \cos^2\theta\dfrac{\partial^2 w}{\partial r^2} + \sin^2\theta\left(\dfrac{1}{r}\dfrac{\partial w}{\partial r} + \dfrac{1}{r^2}\dfrac{\partial^2 w}{\partial\theta^2}\right) + 2\sin\theta\cos\theta\left(\dfrac{1}{r^2}\dfrac{\partial w}{\partial\theta} - \dfrac{\partial^2 w}{r\partial r\partial\theta}\right) \\ \dfrac{\partial^2 w}{\partial y^2} = \sin^2\theta\dfrac{\partial^2 w}{\partial r^2} + \cos^2\theta\left(\dfrac{1}{r}\dfrac{\partial w}{\partial r} + \dfrac{1}{r^2}\dfrac{\partial^2 w}{\partial\theta^2}\right) - 2\sin\theta\cos\theta\left(\dfrac{1}{r^2}\dfrac{\partial w}{\partial\theta} - \dfrac{\partial^2 w}{r\partial r\partial\theta}\right) \\ \dfrac{\partial^2 w}{\partial x\partial y} = \sin\theta\cos\theta\dfrac{\partial^2 w}{\partial r^2} + \dfrac{\cos^2\theta - \sin^2\theta}{r}\dfrac{\partial^2 w}{\partial r\partial\theta} - \dfrac{\sin\theta\cos\theta}{r}\dfrac{\partial w}{\partial r} \\ \qquad - \dfrac{\cos^2\theta - \sin^2\theta}{r^2}\dfrac{\partial w}{\partial\theta} - \dfrac{\sin\theta\cos\theta}{r^2}\dfrac{\partial^2 w}{\partial\theta^2} \end{cases} \tag{7}$$

It is assumed that the piezoelectric thin film sensor model has only radial displacement, no circumferential displacement, but there is circumferential strain. Therefore, the relationship between stress and strain is:

$$\begin{cases} S_{rr} = -z\dfrac{\partial^2 w(r,t)}{\partial r^2} \\ S_{\theta\theta} = -z\dfrac{1}{r}\dfrac{\partial w(r,t)}{\partial r} \end{cases} \tag{8}$$

Where, $S_{rr}$ is the radial strain, $S_{\theta\theta}$ is the tangential strain, and $w(r,t)$ is the neutral axis deflection.

In the thickness direction of the bolt surface, due to the existence of the piezoelectric film sensor, the neutral plane (axis) will change. It can be seen from the position of the coordinate system in Figure 4 that the tangential strain can be ignored. The neutral axis does not change on the external annular surface, and the relationship between stress and strain remains unchanged. For the part with piezoelectric film sensor, the relationship between radial stress and strain is:

$$\begin{cases} S'_{rr} = -(z-h_{lc})\dfrac{\partial^2 w(r,t)}{\partial r^2} \\ S'_{\theta\theta} = -(z-h_{lc})\dfrac{1}{r}\dfrac{\partial w(r,t)}{\partial r} \end{cases} \tag{9}$$

Wherein, $h_{lc}$ is the neutral surface formed after preparing the piezoelectric film sensor.

From the radial balance equation:

$$2\pi r_c \int_{-\frac{h_l}{2}}^{\frac{h_l}{2}} \sigma_r^c(z)dz + 2\pi r_t \int_{-\frac{h_l}{2}}^{\frac{h_l}{2}+h_c} \sigma_r^l(z)dz = 0 \tag{10}$$

Where, $\sigma_r^c$ is the stress on the sensor and $\sigma_r^l$ is the stress on the bolt.

Using Hooke's theorem, equation (10) can be transformed into:

$$r_c \int_{-\frac{h_l}{2}}^{\frac{h_l}{2}} E_c(z-h_{lc})dz + r_t \int_{-\frac{h_l}{2}}^{\frac{h_l}{2}+h_c} E_l(z-h_{lc})dz = 0 \tag{11}$$

Wherein, $E_c$ and $E_l$ are Young's modulus of elasticity of sensor and bolt respectively.

After simplifying formula (11), the expression of neutral axis $h_{lc}$ can be obtained:

$$h_{lc} = \frac{r_t E_l h_c (h_c + h_l)}{2(r_t E_l h_c + r_c E_c h_l)} \tag{12}$$

The potential energy of the smart bolt head is divided into the piezoelectric film sensor part and the outer ring sensor free part, which are expressed in sections according to the integral in Formula (1):

$$\delta U = \int_{r_c}^{r_t}\int_0^{2\pi}\int_{-\frac{h_l}{2}}^{\frac{h_l}{2}} \left(E_l S_{rr}\delta S_{rr}\right) rdrd\theta dz + \int_0^{r_c}\int_0^{2\pi}\int_{-\frac{h_l}{2}}^{\frac{h_l}{2}} \left(E_l S_{rr}\delta S_{rr}\right) rdrd\theta dz +$$
$$\int_0^{r_c}\int_0^{2\pi}\int_{\frac{h_l}{2}}^{\frac{h_l}{2}+h_c} \left\{\left(E_c S_{rr}^{'} - h_{31}D_3\right)\delta S_{rr} + \left(-h_{31}S_{rr}^{'} + \beta_{33}^{S}D_3\right)\delta D_3\right\} rdrd\theta dz \quad (13)$$

Substitute Eq. (8) and Eq. (9) into Eq. (13) to get:

$$\delta U = \int_0^{r_t}\left\{ g(r)\frac{\partial^2 w(r,t)}{\partial r^2}\delta\left(\frac{\partial^2 w(r,t)}{\partial r^2}\right) + \beta_s D_3(r,t)\delta D_3(r,t) + \right.$$
$$\left. h_s\frac{\partial^2 w(r,t)}{\partial r^2}\delta D_3(r,t) + h_s D_3(r,t)\delta\left(\frac{\partial^2 w(r,t)}{\partial r^2}\right)\right\} dr \quad (14)$$

Where, $g(r) = \frac{2\pi}{3}\left\{\frac{E_l h_l^3}{4} + \left[3E_l h_l h_{lc}^2 + E_c h_c^3 + 3E_c h_c\left(\frac{h_l}{2} - h_{lc}\right)^2 + 3h_c^2\left(\frac{h_l}{2} - h_{lc}\right)\right]\right\}$,

$h_s = \pi r h_{31} h_c\left(h_c + h_l - 2h_{lc}\right)$, $\beta_s = \beta_{33}^{s} 2\pi r h_c$ 。

Similarly, the kinetic energy expression of the smart bolt model can be obtained:

$$T = \frac{1}{2}\int_{r_c}^{r_t} \pi\rho_l h_l\left(r_t^2 - r_c^2\right)\left[\frac{\partial w(r,t)}{\partial r}\right]^2 dr + \frac{1}{2}\int_0^{r_c} \pi r_c^2\left(\rho_c h_c + \rho_l h_l\right)\left[\frac{\partial w(r,t)}{\partial r}\right]^2 dr$$
$$= \frac{1}{2}\pi\int_0^{r_t} \rho(r)\left[\frac{\partial w(r,t)}{\partial r}\right]^2 dr \quad (15)$$

Where, $\rho(r) = \rho_l h_l\left(r_t^2 - r_c^2\right) + r_c^2\left(\rho_c h_c + \rho_l h_l\right) = r_t^2\rho_l h_l + r_c^2\rho_c h_c$ , $\rho_l$ is the density of the bolt, $\rho_c$ is the density of piezoelectric material。

The kinetic energy formula (15) is converted into the virtual work expression as follows:

$$\delta T = \pi\int_0^{r_t} \rho(r)\frac{\partial w(r,t)}{\partial r}\delta\left[\frac{\partial w(r,t)}{\partial r}\right] dr \quad (16)$$

Considering the viscous damping of materials and structural damping, the mechanical virtual work of smart bolts is:

$$\delta W_m^{wl} = -B\int_0^{r_t}\left[\frac{\partial w(r,t)}{\partial r}\right]\partial w(r,t)dr - C\int_0^{r_t}\left[\frac{\partial^2 w(r,t)}{\partial r\partial t}\right]\partial w(r,t)dr \quad (17)$$

where, $B$ is viscous damping, $C$ is structural damping。

The electric virtual work of piezoelectric film due to loading is:

$$\delta W_e^{wl} = 2\pi r_c \int_0^{r_c} V_a(r,t)\delta D_3(r,t)\,dr \tag{18}$$

Extended Hamilton principle formula:

$$\int_{t_1}^{t_2} \left(\delta L + \delta W^{wl}\right) dt = 0 \tag{19}$$

Where, Lagrangian function $\delta L = \delta T - \delta U$ and virtual work $\delta W^{wl} = \delta W_m^{wl} + \delta W_e^{wl}$ generated by external force.

Substitute equations (14), (16), (17) and (18) into equation (19) to obtain:

$$\int_{t_1}^{t_2} \left\{ \pi \int_0^{r_t} \rho(r) \frac{\partial w(r,t)}{\partial r} \delta\left[\frac{\partial w(r,t)}{\partial r}\right] dr - \int_0^{r_t} \left\{ g(r) \frac{\partial^2 w(r,t)}{\partial r^2} \delta\left(\frac{\partial^2 w(r,t)}{\partial r^2}\right) + \right.\right.$$
$$\left.\beta_s D_3(r,t)\delta D_3(r,t) + h_s \frac{\partial^2 w(r,t)}{\partial r^2}\delta D_3(r,t) + h_s D_3(r,t)\delta\left(\frac{\partial^2 w(r,t)}{\partial r^2}\right)\right\} dr +$$
$$\left. 2\pi r_c \int_0^{r_c} V_a(r,t)\delta D_3(r,t)\,dr - B\int_0^{r_t}\left[\frac{\partial w(r,t)}{\partial r}\right]\partial w(r,t)\,dr - C\int_0^{r_t}\left[\frac{\partial^2 w(r,t)}{\partial r \partial t}\right]\partial w(r,t)\,dr \right\} dt \tag{20}$$

Transforming equation (20), we can get:

$$\int_{t_1}^{t_2} \left\{ \int_0^{r_t} \left[ \left( -\rho(r) \frac{\partial^2 w(r,t)}{\partial t^2} - \frac{\partial}{\partial r}\left( g(r) \frac{\partial^2 w(r,t)}{\partial r^2} \right) - h_s \frac{\partial^2 D_3(r,t)}{\partial r^2} - \right.\right.\right.$$
$$\left. B\frac{\partial w(r,t)}{\partial t} - C\frac{\partial^2 w(r,t)}{\partial r \partial t} \right)\delta w(r,t) + \left(-\beta_s D_3(r,t) - h_s \frac{\partial^2 w(r,t)}{\partial r^2} + \right.$$
$$\left.\left. 2\pi r V_a(r,t)\right)\delta D_3(r,t)\right] dr - \left( g(r)\frac{\partial^2 w(r,t)}{\partial r^2} + h_s D_3(r,t)\right)\delta\left(\frac{\partial w(r,t)}{\partial r}\right)\Bigg|_0^{r_t} -$$
$$\left.\left[\frac{\partial}{\partial r}\left( g(r)\frac{\partial^2 w(r,t)}{\partial r^2}\right) + h_s \frac{\partial D_3(r,t)}{\partial r}\right]\delta w(r,t)\Bigg|_0^{r_t}\right\} dt = 0 \tag{21}$$

Since the variable change in equation (21) is not affected by $\delta w(r,t)$ and $\delta D_3(r,t)$, its coefficient is zero. The equation can be obtained:

$$\beta_s D_3(r,t) + h_s \frac{\partial^2 w(r,t)}{\partial r^2} = 2\pi r V_a(r,t) \tag{22}$$

Equation (22) reflects the static coupling relationship between the bolt surface and the piezoelectric film sensor.

## 3. Simulation model and operation steps

### 3.1. Simulation model

The object of this paper is the assembly model of single bolt structure, as shown in Figure 6. CAXA solid design is used to complete the creation of 3D model and import it into Comsol software. In order to improve the accuracy of simulation, the three-dimensional model is the same size as the experiment. The simulation in this section focuses on the stress on the surface of the bolt head. Higher excitation frequencies are difficult to transmit to the connecting plate.

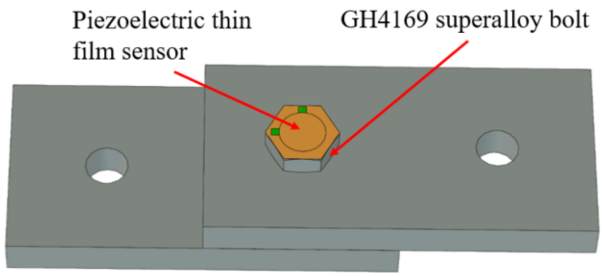


**Figure 6** Three-dimensional model of single bolt simulation

### 3.2. Operating steps

(1) Parameter setting

After importing the model, set the relevant materials. The piezoelectric film sensor is ZnO, the bolt is GH4169 high temperature alloy steel, and the connecting plate is Q345 steel plate. Its parameters are shown in Table 1 and Table 2.

**Table 1.** Simulation parameters of piezoelectric materials

| Parameter | Value |
|---|---|
| Piezoelectric flexibility matrix ( $m^2 / N$ ) | $\begin{pmatrix} 20.97 & 12.11 & 10.51 & 0 & 0 & 0 \\ 12.11 & 20.97 & 10.51 & 0 & 0 & 0 \\ 10.51 & 10.51 & 21.09 & 0 & 0 & 0 \\ 0 & 0 & 0 & 4.43 & 0 & 0 \\ 0 & 0 & 0 & 0 & 4.24 & 0 \\ 0 & 0 & 0 & 0 & 0 & 4.24 \end{pmatrix} \times 10^{12}$ |
| Piezoelectric stress constant matrix ( $C / m^2$ ) | $\begin{pmatrix} 0 & 0 & 0 & 0 & -11.34 & 0 \\ 0 & 0 & 0 & -11.34 & 0 & 0 \\ -5.43 & -5.43 & 11.67 & 0 & 0 & 0 \end{pmatrix} \times 10^{-12}$ |
| Relative dielectric matrix | $\begin{pmatrix} 8.55 & 0 & 0 \\ 0 & 8.55 & 0 \\ 0 & 0 & 8.55 \end{pmatrix}$ |
| Elastic modulus ( $GPa$ ) | 110-140 |
| Density $\rho$ ( $kg / m^3$ ) | $5.61 \times 10^3$ |
| Dielectric constant | 8.66 |

**Table 2.** Simulation parameters of ZnO piezoelectric thin films

| | Material | Elastic modulus $GPa$ | Density $kg/m^3$ | Poisson's ratio |
|---|---|---|---|---|
| Bolt | GH4169 | 199.9 | 8240 | 0.3 |
| Protective layer/insulation layer | $SiO_2$ | 73 | 2230 | 0.2 |
| electrode | NiCr | 60 | 8400 | 0.2 |

(2) Physical field settings

After completing the 3D model import and material attribute setting, complete the boundary setting, bolt pre tightening force operation and continuity operation necessary for simulation, as shown in Figure 7. Open the solid mechanics module and set the piezoelectric properties of the piezoelectric film sensor, so that the piezoelectric partial differential equation will take effect in the sensor area. Then, set the contact surface between the bolt head and the connecting plate in Figure 6 as relative sliding. The augmented Lagrangian method is used to solve the problem. The initial value of the contact pressure is. The contact pair is added to the contact sub column of solid mechanics and takes effect. At the same time, the consistent pair is added to the continuous sub column. The lower end face of the nut is adjusted as a fixed constraint, and the bolt rod is adjusted as a spring property, which can effectively ensure the convergence of the augmented Lagrangian calculation.

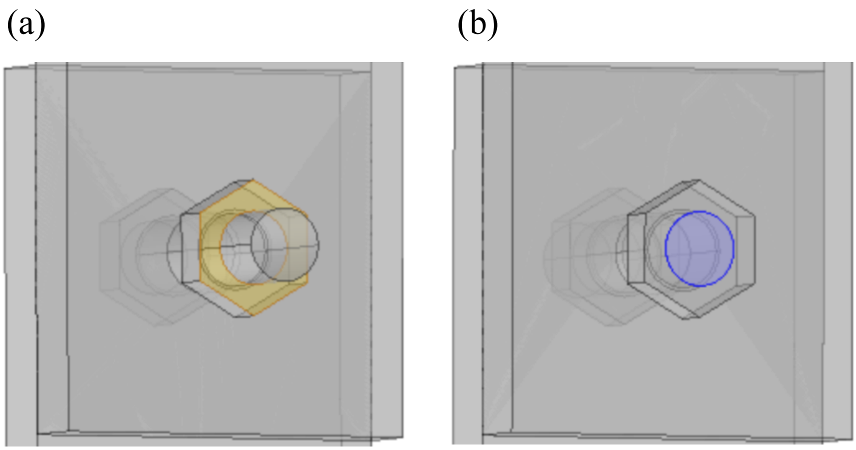


**Figure 7**. Fixed constraint of nut lower end face and piezoelectric property setting of piezoelectric thin film sensor

During the simulation operation, the nodes are set with the preload parameters provided by the software for scanning. Then use the cross section set in advance in the bolt, as shown in green in Figure 8 (a), and the applied pre tightening force is set mainly through this section, which can make the bolt produce tensile stress while exerting pressure on the coupling plate. In addition, the spring condition is set at the bottom of the bolt, as shown in Figure 8 (b).

After the mechanical setting of the mechanical part is completed, the electrical module is further set to make the piezoelectric film sensor have piezoelectric characteristics. Open the electrostatic module, apply electric field to the piezoelectric sensor, set the upper surface as voltage, and use the Linper() function to set the voltage value as 0.2V. Set the lower surface of the piezoelectric sensor to zero potential, as shown in Figure 9.

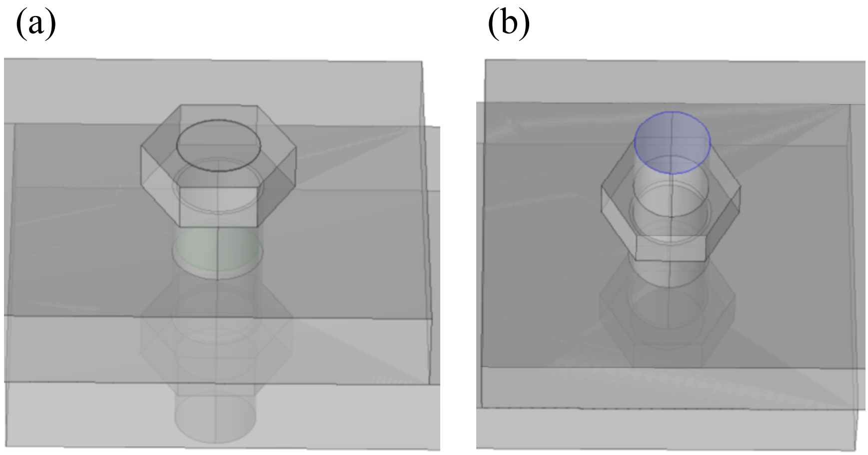


**Figure 8.** Bolt axial preload section and bolt spring condition

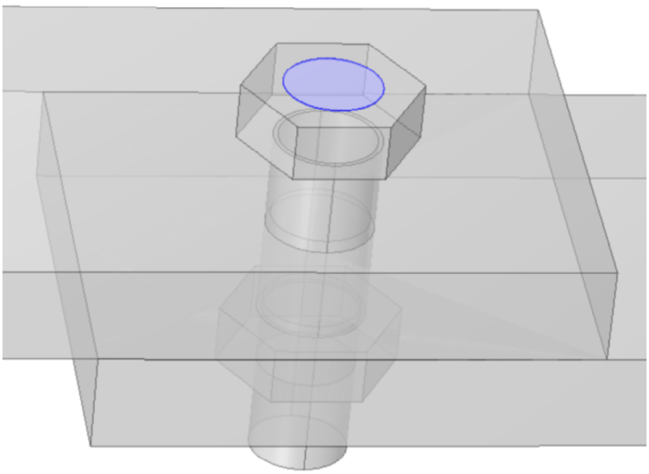

**Figure 9.** Electrical setting of piezoelectric thin film sensor

(3) Gridding

After the solid mechanics and electricity settings are completed, the model needs to be meshed, the area to be analyzed needs to be miniaturized, and the structure is calculated in this way. Of course, the smaller the micro cells are divided, the closer the result obtained after merging is to the true value. However, the finer the grid is, the higher the computing capacity of the computer is required. At the same time, it may be difficult to converge. Therefore, the grid division shall be determined based on the comprehensive consideration of solution accuracy and laboratory computer ability.

During the axial preload test of the bolt, the natural frequency of the bolt needs to be scanned in advance. The relationship between the wavelength and the maximum grid size is as follows:

$$l_{mesh} < \frac{v}{3f_{\max}} \quad (23)$$

Where, $l_{mesh}$ is the maximum size of the grid, $v$ is the speed of sound propagation in the structure, and $f_{\max}$ is the voltage frequency excited during scanning. The maximum frequency selected in this section is 0.9215 MHz, and the sound velocity in steel is $5920m/s$. According to Formula (23), the maximum grid size is 2.14 mm.

The software provides quadrilateral, hexahedron, tetrahedron, triangle and other mesh elements. The mesh division required by the model can be obtained by using free mesh, swept mesh and mapped mesh. In this section, the piezoelectric film sensor, bolt head and bolt rod are meshed manually, and then the operation is completed by sweeping. The result after partition is shown in Figure 10.

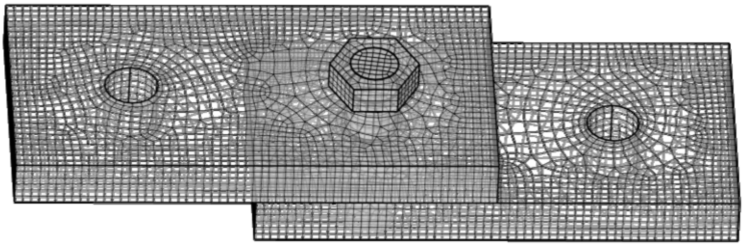

**Figure 10.** Results of model mesh generation

### *3.3. Piezoelectric response of ZnO piezoelectric thin film sensor*

In order to study the relationship between the peak admittance frequency (impedance) of the smart bolt and the axial preload of the bolt, it is necessary to scan the frequency of the smart bolt when it is not loaded to determine the range of its peak admittance. The scanning frequency range is 0.6MHz~1.0MHz, and the step size is 100Hz. The scanning results are shown in Figure 11.

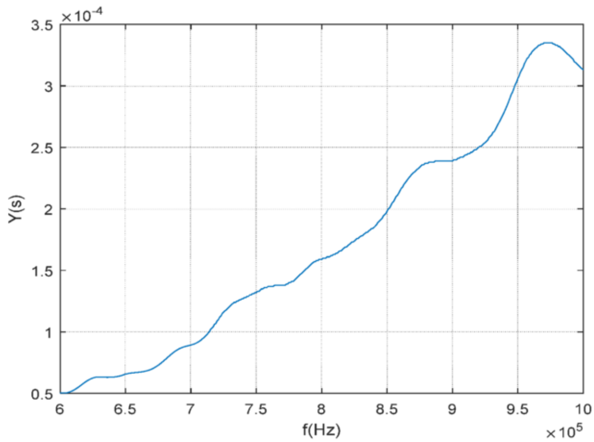


**Figure 11.** Coarse frequency scanning results of intelligent bolt admittance

It can be seen from the figure that there is a strong admittance peak near 0.972MHz. It is fixed to set 0.95MHz~1.0MHz as the frequency band for simulation research, and the step size is 100Hz. With the theoretical derivation results as reference, the minimum torque in the simulation process is. At this time, the obtained admittance results are shown in Figure 12.

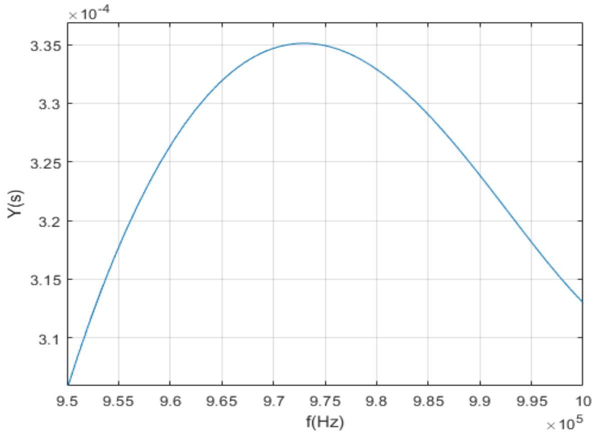


**Figure 12.** Admittance diagram at torque of $15N \cdot m$

## 4. Simulation results and discussion

### *4.1. Effects of different piezoelectric materials*

ZnO, AlN, and PZT are commonly used materials in preparing piezoelectric thin film sensors. Therefore, this paper uses comsol software to simulate the piezoelectric properties of piezoelectric materials before the preparation of smart bolts, in order to guide the experiment. The output characteristics of voltage and impedance of the three piezoelectric materials with the same size and the same parameter settings under excitation frequency are studied respectively, as shown in Figure 13.

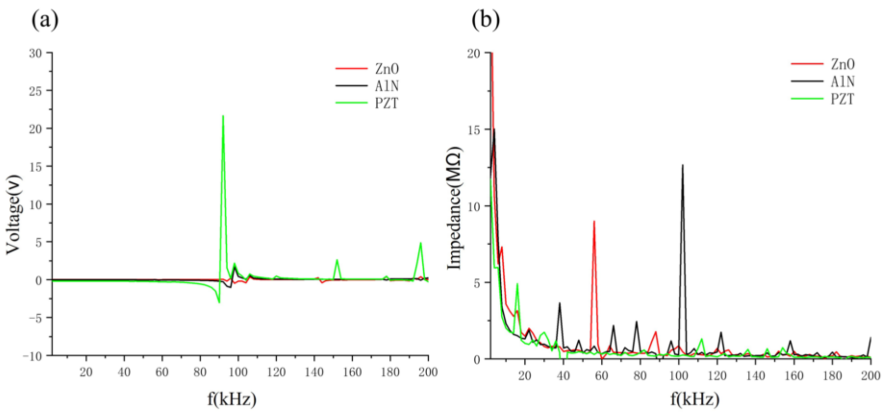


**Figure 13.** Schematic diagram of positive piezoelectric effect

Figure 13 (a) shows the output voltage of three piezoelectric materials at the excitation frequency. It can be seen that under the same excitation frequency, the output voltage value of PZT is much higher than that of the other two materials, and the output voltage values of ZnO and AlN are relatively close. The output voltage of piezoelectric materials is mainly related to the piezoelectric coefficient, which is also consistent with the literature. Figure 13 (b) shows the impedance changes of the three materials at the excitation frequency, with the highest AlN and the lowest PZT.

According to the comprehensive consideration of laboratory experimental conditions and simulation results, although PZT has the strongest piezoelectric output performance, its preparation requirements are high, the proportion of multiple materials is difficult to control, and ultimately it is difficult to achieve the ideal piezoelectric output. AlN materials require high vacuum when preparing piezoelectric films, and AlON is easy to form in actual preparation. Finally, ZnO is selected as the piezoelectric material of piezoelectric thin film sensor.

### *4.2. Influence of piezoelectric material shape*

Piezoelectric thin film sensor is prepared at the head of the bolt. Since the bolt head is circular, the piezoelectric thin film sensor is also considered to be circular, but the selection of solid circle or circular ring needs to be verified through simulation to reduce the experimental workload. According to the actual diameter of bolt head (16mm), the specific dimensions of circular and annular piezoelectric materials are selected as shown in Figure 14.

It can be seen from Figure 15 (a) that the output voltage of circular piezoelectric materials is much greater than that of rings, which also reflects that circular piezoelectric materials will generate more charges when they are excited. Fig. 15 (b) shows that the amplitude of annular impedance is greater than that of circular impedance, that is, the amplitude of impedance increases when the area decreases [15]. In addition, considering the difficulty of the preparation process of the circle and the ring, this paper chooses the circle as the shape of the experiment.

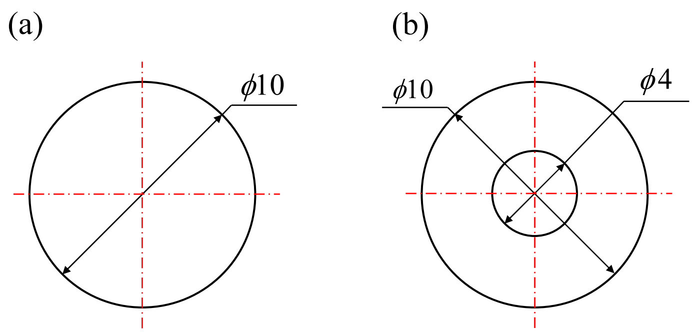


**Figure. 14.** Piezoelectric material shape: (a) circular, (b) annular

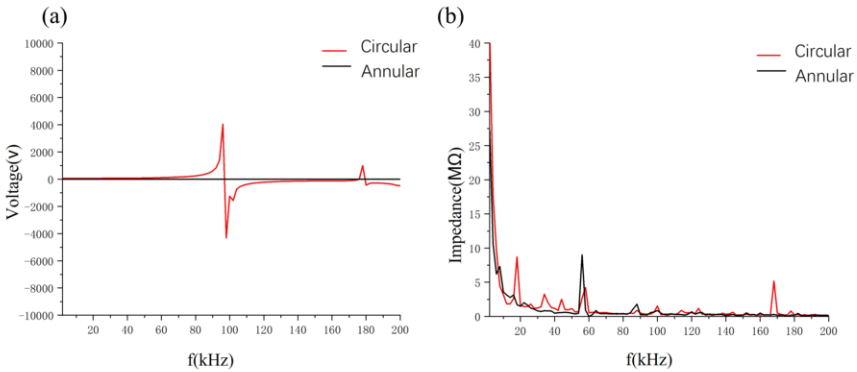


**Figure. 15.** Output voltage and impedance characteristics of circular and annular piezoelectric materials under excitation frequency

## 4.3. Piezoelectric material size effect

In this paper, the piezoelectric film sensors with diameters of 6mm, 8mm, 10mm and 12mm are selected to analyze the output voltage and impedance curves of piezoelectric film sensors with different sizes, as shown in Figure 16. Figure 16 (a) shows that the output voltage of piezoelectric film sensor increases with the increase of diameter under different diameters. Figure 16 (b) shows that the smaller the diameter, the greater the impedance of the piezoelectric film sensor, which is consistent with the theoretical model of energy trapping [16]. Considering the variation curve of voltage output and impedance and the limitation of bolt head surface size, the diameter of piezoelectric material selected in this paper is 10mm.

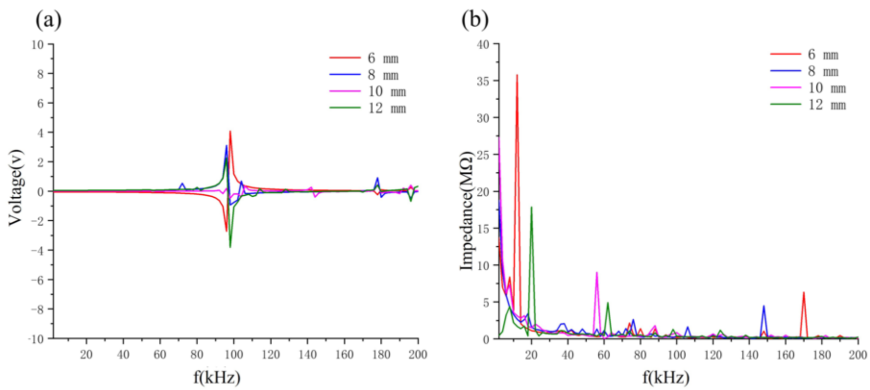


**Figure. 16.** Output voltage and impedance characteristics of piezoelectric materials *with different sizes under excitation frequency*

## 4.4. Influence of piezoelectric material thickness

In order to study the influence of the film thickness on the output voltage and impedance of the piezoelectric film sensor, Comsol software is used to simulate and analyze the piezoelectric material thickness of 600nm, 800nm, 1000nm and 1200nm.

The results are shown in Figure 17. Figure 17 (a) shows that the output voltage of the sensor increases with the increase of the film thickness. Figure 17 (b) shows that when the thickness is 1200nm, the impedance is large, which exceeds the legend. However, with the increase of film thickness, the film tends to peel. Therefore, 1000 nm is selected as the thickness of the sensor in this paper.

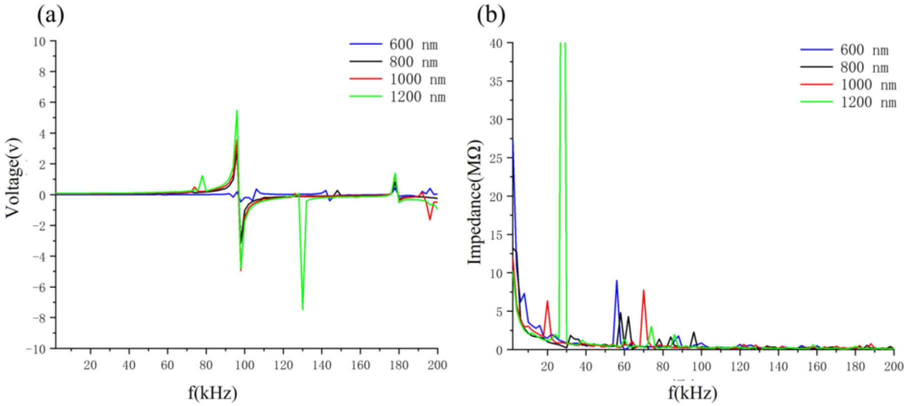


**Figure 17.** Output voltage and impedance characteristics of piezoelectric materials with different thickness under excitation frequency

## 4.5. *Effect of electrode material size*

Because the process for preparing NiCr in the laboratory has been mature, NiCr is selected as the electrode material in this paper. According to the size of piezoelectric film, study the effect of electrode size on voltage output and impedance change. Select the electrode material size and choose the diameter of 4mm, 6mm and 8mm for research. The results are shown in Figure 18. When the electrode size is 6mm, the piezoelectric thin film sensor has a higher output voltage. At this time, when the impedance value is large, the piezoelectric impedance frequency is small. Therefore, 6mm is selected as the experimental electrode size in this paper.

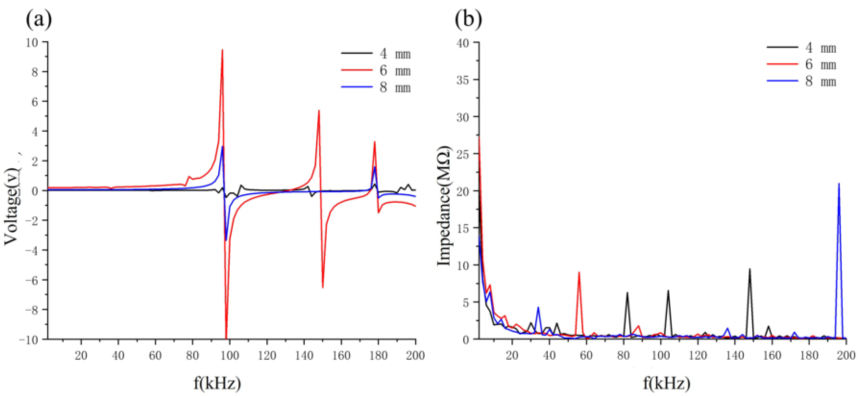


**Figure 18.** Output voltage and impedance characteristics of different size electrodes under excitation frequency

### 4.6. Influence of electrode material thickness

After the electrode size is determined, it is necessary to study the electrode thickness and select the appropriate thickness. Three thicknesses with diameters of 100nm, 200nm and 300nm were selected for analysis, and the results are shown in Figure 19. Figure 19 (a) shows the output voltage under three electrode thicknesses. When the electrode thickness is 100nm, the maximum output voltage is obtained. Figure 19 (b) shows the change of output impedance under three electrode thicknesses. The electrode thickness of 300 nm has the maximum output impedance. The thickness of electrode material will generate heat due to its ohmic effect, which will affect the adhesion of devices. Therefore, 200nm is selected as the electrode thickness for the experiment.

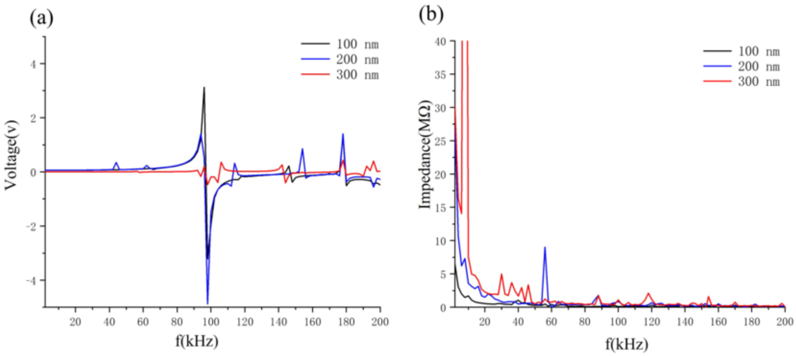


**Figure 19.** Output voltage and impedance characteristics of different electrode thickness under excitation frequency

## 5. Conclusions

The solid mechanical field and electrical field of the smart bolt are established by Comsol Multiphysic software, and the natural resonance frequency of the smart bolt is roughly scanned to confirm the approximate range of the admittance peak frequency. Through the simulation of each film layer of piezoelectric thin film sensor, it can be concluded that the piezoelectric material is ZnO, the piezoelectric material is circular in shape, the piezoelectric material size is 10mm, the piezoelectric material thickness is 1000nm, the electrode material size is 6mm, and the electrode thickness is 200nm. ZnO piezoelectric thin film sensor was fabricated with this material and size.

## Acknowledgments

This work was supported by the National Natural Science Foundation of China (No. 51905071), The National Natural Science Foundation of China (No. 52175379), Research of the Education, Department of Liaoning Province (No. LJKZ0483), Scientific Research Fund Project of Liaoning, Provincial Department of Education (IX202005), Scientific Research Project of Liaoning Machinery, Electricity Vocational Technical College (KY202004).

## Reference


[1] Zhao N, Huo L, Song G. A nonlinear ultrasonic method for real-time bolt looseness monitoring using PZT transducer–enabled vibro-acoustic modulation. Journal of Intelligent Material Systems and Structures, 2019,31(3): 364-376.

[2] Wang F, Song G. Bolt early looseness monitoring using modified vibro-acoustic modulation by time-reversal. Mechanical Systems and Signal Processing, 2019,130: 349-360.

[3] Zhang M, Shen Y, Xiao L, et al. Application of subharmonic resonance for the detection of bolted joint looseness. Nonlinear Dynamics, 2017,88(3): 1643-1653.

[4] Zhang Z, Liu M, Su Z, et al. Quantitative evaluation of residual torque of a loose bolt based on wave energy dissipation and vibro-acoustic modulation: A comparative study. Journal of Sound and Vibration, 2016,383: 156-170.

[5] Yuan R, Lv Y, Wang T, et al. Looseness monitoring of multiple M1 bolt joints using multivariate intrinsic multiscale entropy analysis and Lorentz signal-enhanced piezoelectric active sensing. Structural Health Monitoring, 2022.

[6] Jiang J, Chen Y, Dai J, et al. Multi-bolt looseness state monitoring using the recursive analytic based active sensing technique. Measurement, 2022,191.

[7] Kim Y-S, Na W S. Development of a portable damage detection system based on electromechanical impedance technique for monitoring of bolted joint structures. Journal of Intelligent Material Systems and Structures, 2022.

[8] Zhou L, Chen S-X, Ni Y-Q, et al. EMI-GCN: a hybrid model for real-time monitoring of multiple bolt looseness using electromechanical impedance and graph convolutional networks. Smart Materials and Structures, 2021,30(3).

[9] Chen L, Xiong H, Yang Z, et al. Preload measurement of steel-to-timber bolted joint using piezoceramic-based electromechanical impedance method. Measurement, 2022,190.

[10] Huo L, Chen D, Liang Y, et al. Impedance based bolt pre-load monitoring using piezoceramic smart washer. Smart Materials and Structures, 2017,26(5).

[11] Wang B, Huo L, Chen D, et al. Impedance-Based Pre-Stress Monitoring of Rock Bolts Using a Piezoceramic-Based Smart Washer-A Feasibility Study. Sensors (Basel), 2017,17(2).

[12] Xingliang H, Yixiang D, Qingwen F, et al. Correction of coupling error in contact-type ultrasonic evaluation of bolt axial stress. Ultrasonics, 2022,124(2022): 106763.

[13] Sun Q, Yuan B, Mu X, et al. Bolt preload measurement based on the acoustoelastic effect using smart piezoelectric bolt. Smart Materials and Structures, 2019,28(5): 107626.R107621-107626.R107617.

[14] Ren L, Feng T, Ho M, et al. A smart "shear sensing" bolt based on FBG sensors. Measurement, 2018,122: 240-246.

[15] Tiersten H F, Stevens D S. An analysis of thickness-extensional trapped energy resonant device structures with rectangular electrodes in the piezoelectric thin film on silicon configuration. Journal of Applied Physics, 1983,54(10): 5893-5910.

[16] H. T F. Analysis of Trapped Energy Resonators Operating in Overtones of Coupled Thickness-Shear and Thickness-Twist. The Journal of the Acoustical Society of America, 1976,59(4): 879-888.